



Chemical gradients in automotive Cu-SSZ-13 catalysts for NO_x removal revealed by operando X-ray spectrotomography

Johannes Becher ¹, Dario Ferreira Sanchez ², Dmitry E. Doronkin^{1,3}, Deniz Zengel¹, Debora Motta Meira ^{4,5,6}, Sakura Pascarelli^{4,7}, Jan-Dierk Grunwaldt ^{1,3} and Thomas L. Sheppard ^{1,3} □

Nitrogen oxide (NO_x) emissions are a major source of pollution, demanding ever-improving performance from catalytic after-treatment systems. However, catalyst development is often hindered by limited understanding of the catalyst at work, exacerbated by widespread use of model catalysts rather than technical catalysts, and by global rather than spatially resolved characterization tools. Here we combine operando X-ray absorption spectroscopy with microtomography to perform three-dimensional chemical imaging of the chemical state of copper species in a Cu-SSZ-13 washcoated monolith catalyst during NO_x reduction. Gradients in copper oxidation state and coordination environment, resulting from an interplay of NO_x reduction with adsorption-desorption of NH₃ and mass transport phenomena, were revealed at micrometre spatial resolution while simultaneously determining catalytic performance. Crucially, direct three-dimensional visualization of complex reactions on non-model catalysts is feasible only by the use of operando X-ray spectrotomography, which can improve our understanding of structure-activity relationships, including the observation of mass and heat transport effects.

ue to health and environmental concerns, there is currently a strong societal demand for improved air quality, driving strict emission limits for CO, nitrogen oxide (NO_x), unburnt hydrocarbons and particulates. The primary means of mitigating such pollutants is through the adoption of more efficient catalytic converters. Highly effective Cu-zeolite catalysts such as Cu-SSZ-13 (Cu-chabazite) are among the prominent recent examples of active materials available for selective catalytic reduction of NO_x with ammonia (NH3-SCR)1,2. Numerous theoretical and experimental studies have aimed to understand the mechanism of NH3-SCR on Cu-chabazites on the molecular scale³⁻⁸. Notably, X-ray absorption spectroscopy (XAS) and infrared spectroscopy have been particularly successful in probing the structure and coordination of potentially active metal species, as well as adsorbates and surface chemistry, respectively. However, NH₃-SCR is a complex process involving variable Cu speciation and temperature-dependent reaction paths⁹, further influenced by the NH₃ adsorption equilibrium¹⁰, including NH₃ inhibition at low temperature^{11–14}. In particular, there is currently no consensus on the nature of the active site at elevated temperatures since this also depends on the positions and local concentrations of NH₃, NO and NO₂ in the catalyst bed. For example, both Cu(I) and Cu(II) species have been reported in the literature predominantly at elevated temperatures 1,3,8,9,13,14. To shed light on catalyst structure, it is thus necessary to perform in situ-preferentially operando-studies under realistic reaction conditions (atmosphere, granulated catalyst) and coupled with catalytic performance measurements. However, despite being very demanding, spatiotemporal effects also need to be considered in the case of temperature or

concentration gradients¹⁵⁻¹⁸. This is because modern emission control systems, such as porous catalyst washcoats on monolith carriers, are structurally fairly complex. Although studies based on plug flow reactors with granulated catalysts^{14,16,18} or self-supported wafers^{3,4} may facilitate data interpretation, such samples can be considered as unrealistic compared to typical technical catalysts—for example, washcoated monoliths. In terms of catalyst form, this oversimplification risks hiding the presence of local structural effects, which is particularly relevant when using global analytical methods such as XAS. In cases such as NH₃-SCR, the catalytic converter optimally needs to be considered while at work, in a spatially resolved manner and on the molecular, meso- and macroscales.

In practice, in situ or operando characterization of non-model catalysts is challenging. While molecular modelling combined with multi-scale simulations can virtually predict reaction steps, surface coverage and concentration of reactants and products in specific volumes of a technical catalyst, for example, ideally experimental data are required to validate such models 19,20. Deviations in measured and predicted activity may indicate mass transport limitations—for example, a slow effective diffusion of reactant and/or product gases in the solid catalyst²¹, which can manifest as gradients within the catalyst particles. Although relatively simple to diagnose, precise characterization of such effects can be difficult—and especially difficult to control solely by optimization of the catalyst design or simulation of reaction behaviour²². To tackle this challenge of spatially resolved characterization, an ideal toolkit has emerged in the form of hard X-ray computed tomography performed at synchrotron light sources. The basis of X-ray computed tomography is

¹Institute for Chemical Technology and Polymer Chemistry, Karlsruhe Institute of Technology, Karlsruhe, Germany. ²Paul Scherrer Institut, Villigen, Switzerland. ³Institute of Catalysis Research and Technology, Karlsruhe Institute of Technology, Eggenstein-Leopoldshafen, Germany. ⁴European Synchrotron Radiation Facility, Grenoble, France. ⁵Present address: Advanced Photon Source, Argonne National Laboratory, Argonne, IL, USA. ⁶Present address: Canadian Light Source Inc., Saskatoon, Saskatchewan, Canada. ¹Present address: European XFEL GmbH, Schenefeld, Germany.

[™]e-mail: grunwaldt@kit.edu; thomas.sheppard@kit.edu

the non-invasive imaging of the interior sample structure, allowing detection and co-localization of sample constituents often at microor nanometre-scale, three-dimensional (3D) spatial resolution²³. X-ray computed tomography can be coupled with various contrasts such as X-ray absorption, fluorescence or diffraction, producing highly spatially resolved chemical data that are unobtainable by contemporary methods²⁴⁻²⁸. This has been elegantly demonstrated, for example, for exhaust gas monoliths^{29,30}, fluid catalytic cracking particles^{25,31} and Ziegler-Natta catalysts³². However, performing operando X-ray computed tomography remains a considerable challenge requiring at least micrometre-scale mechanical precision in 3D, free rotation of the reactor and unhindered X-ray transmission around 180°, maintaining reaction conditions and, ideally, simultaneous measurement of catalytic activity. Several cutting-edge studies on powdered or pelletized catalysts at work (that is, model systems) have been published on Fischer-Tropsch synthesis³³⁻³⁵, oxidative coupling of methane^{36,37} and partial methane oxidation³⁸. However, complex, hierarchically structured systems such as exhaust gas catalysts have not been investigated. In particular, quantitative catalytic activity data, which are crucial for accurate assessment of structureactivity relationships, have not been reported to date. Notably, the location and speciation of Cu in Cu-SSZ-13 catalysts has previously been explored at nanometre resolution by an alternative 3D imaging method known as atom probe tomography^{39,40}. However, because this method is completely destructive and operates in a high vacuum, it cannot be exploited for operando studies. Complementary sample-preserving methods are highly desirable, particularly in catalysis research.

Here we introduce operando hard X-ray spectrotomography applied to a complex emissions control process, Cu-SSZ-13-catalysed NH₃-SCR, on a washcoated monolithic catalyst. Using a dedicated sample environment for operando tomography, we combined XAS and X-ray CT for spatially and energy-resolved 3D imaging at the Cu K-edge, coupled to quantitative catalytic performance data. Probing the catalyst under NH₃-SCR conditions at 200–400 °C revealed clear chemical gradients of the Cu oxidation state and degree of NH₃ coordination within the Cu-SSZ-13 washcoat. Crucially, we show that direct, semi-quantitative observation of chemical gradients as a function of temperature and washcoat structure is uniquely possible with operando spectrotomography. As demonstrated here for automotive catalysis, the method is applicable for a variety of technical catalysts and functional materials.

Results

Monolith preparation and NH₃-SCR reaction conditions. Coated monolithic NH3-SCR catalysts were prepared by washcoating Cu-SSZ-13 (1.8 wt% Cu) onto a cordierite honeycomb substrate with square channels (~1.27 mm edge length). Single monolithic channels and channel corners (length ~5 mm) were carefully extracted using a razor blade, without damaging the washcoat, and placed within the spectrotomography reactor (Supplementary Methods). Standard SCR conditions (1,000 ppm NO, 1,000 ppm NH₃, 7.8% O₂ in He, total flow 50 ml min⁻¹) were maintained while varying the temperature from 200 to 400 °C using hot-air blowers over a period of 50 h. Reference conditions were also measured, including 1,000 ppm NH₃ in He (NH₃-only reference) and 1,000 ppm NO with 7.8% O_2 in He (NO-only reference). NO conversion and N_2 yield were analysed by a mass spectrometer positioned downstream from the reactor. The high gas hourly space velocity, together with high gas bypass through the monolith channel void, limited NO conversion to approximately 10%. This allowed the assumption of a relatively uniform gas composition throughout the catalyst bed (for example, maximum possible gradient of NH₃ and NO from 1,000 to 900 ppm along the reactor), and therefore an expected uniform composition of the catalyst in axial geometry.

Operando spectrotomography of Cu-SSZ-13 monolith. The spectrotomography set-up designed for this study, including an X-ray-transparent support rod for stability (Fig. 1a) was installed at microXAS beamline (Paul Scherrer Institut; Supplementary Methods). An X-ray beam in parallel geometry, with a cross-section of ~1.5×1.0 mm² and energy tuned around the Cu K-absorption edge, was used to acquire full-field projected images of the catalyst monolith. Collecting projection series at 51 different energy points (8,970-9,010 eV), while rotating the sample through an arc of 180°, enabled tomographic data reconstruction with a final 3D spatial resolution of 5 µm (Supplementary Methods). This combination of XAS and 3D imaging is denoted here as spectrotomography. The resulting data volume can be subdivided into cross-sectional images or slices, providing a 3D view of the sample interior. For example, a clear distinction between catalyst washcoat material and cordierite honeycomb was readily observed based on differing absorption contrast (Figs. 1a and 2a,b). Within each slice, each individual pixel consists of an independent X-ray absorption near-edge structure (XANES) spectrum at the Cu K-edge (Fig. 2c). In this way the active metal species could be probed and independently co-located in 3D within the entire technical catalyst under various operando conditions. Note that the pre-edge and edge features at the Cu K-edge are strongly dependent on the oxidation state and, particularly, on the geometry of Cu sites with different probability of 1s-3d and 1s-4p transitions^{41,42}.

As a result of this data collection strategy, distinct gradients in XANES intensity were observed under operando SCR conditions. These manifested in an approximately radial manner, centred on the innermost corner of the washcoat. The gradients were apparently linked to washcoat thickness (Supplementary Discussion) or, conversely, to the distance from the open gas stream in the surrounding capillary (Fig. 1b). This effect was noticeable particularly at 8,983 eV, correlating to the presence of an intense feature commonly observed in Cu(1) species, especially linear Cu(NH₃)₂+ species or similar geometries due to permitted 1s-4p transitions⁴³. The gradients were furthermore linked to temperature and were most visible at >300 °C, correlating with NO conversions of 10-12% (Fig. 1b). In contrast, at 200 °C the gradients were less pronounced, indicating a comparatively uniform state of Cu and lower NO conversion.

3D spatially resolved XANES fitting of Cu-SSZ-13 washcoat. To explain the presence of these chemical gradients according to current understanding of the NH₃-SCR mechanism, XANES fitting and analysis of the entire washcoat material was performed. Although this was possible on a per-pixel basis, several regions of interest (ROI) were defined to improve spectral quality and facilitate image analysis (Fig. 2b). XANES data were extracted in an approximately radial manner, starting from the thickest point of the washcoat at the honeycomb corner (ROI 1) to the washcoat exterior close to the gas stream (ROI 5) (Fig. 2c). ROI 1–5 therefore represent a chemical fingerprint of Cu oxidation state and coordination environment, correlated to increasing diffusion path lengths of reactant or product gas through the washcoat.

Because operando spectrotomography experiments were performed under standard SCR conditions at $\geq 200\,^{\circ}$ C, the most relevant Cu species were considered to be Cu(I) with or without bonded NH₃, along with hydrated and dehydrated Cu(II)^{10,13,44}. Due to variation in both oxidation state and geometry, and thus variation in Cu 1s–4p transition probability, the XANES spectra of these copper species are clearly distinguishable by their form, particularly the feature at 8,983 eV (refs. ^{10,43}). To map the distribution of specific Cu species in the washcoat, linear combination fitting of the measured XANES spectra was performed after ROI selection and normalization (Supplementary Discussion and Supplementary Figs. 4–9). The following four species were selected as references: Cu(I)*NH₃ corresponding to linear Cu(NH₃)₂+; Cu(I) mostly without adsorbed

ARTICLES NATURE CATALYSIS

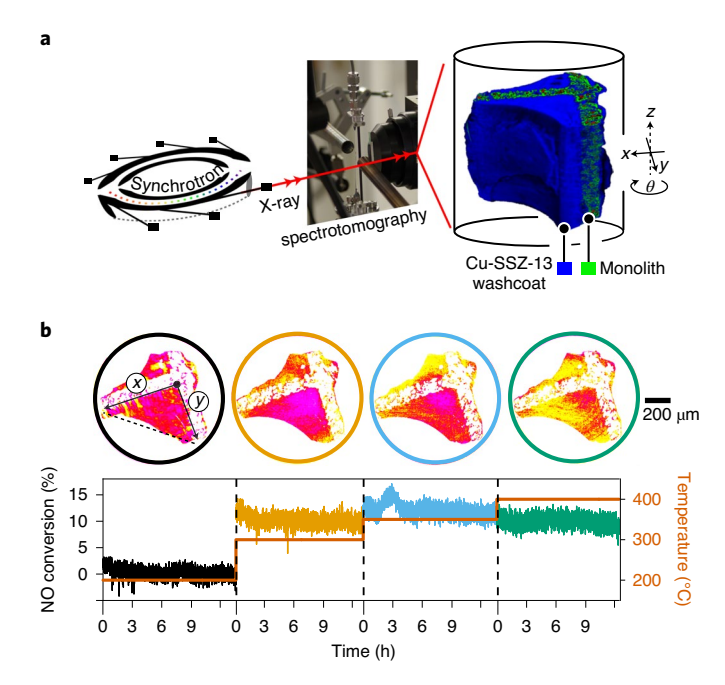


Fig. 1 Operando spectrotomography of a Cu-SSZ-13 catalyst at work. **a**, Sketch of the operando spectrotomography experiment at the microXAS beamline, and tomography rendering of the Cu-SSZ-13 washcoated catalyst. **b**, Orthogonal raw data slices of the catalyst under model SCR conditions—artificially enhanced contrast depicting Cu XANES spectrum intensity at 8,983 eV (for illustration only, and not normalized between datasets)—with truncated mass spectrometry data showing NO conversion during tomography scans at each temperature condition (zero is the time at which the tomography scan was started).

ammonia; hydrated Cu(II) (five-coordinated); and dehydrated Cu(II) (three- or four-coordinated, the spectra of which are highly similar)^{6,10,45}. For further information on selection and acquisition of reference data see Supplementary Discussion.

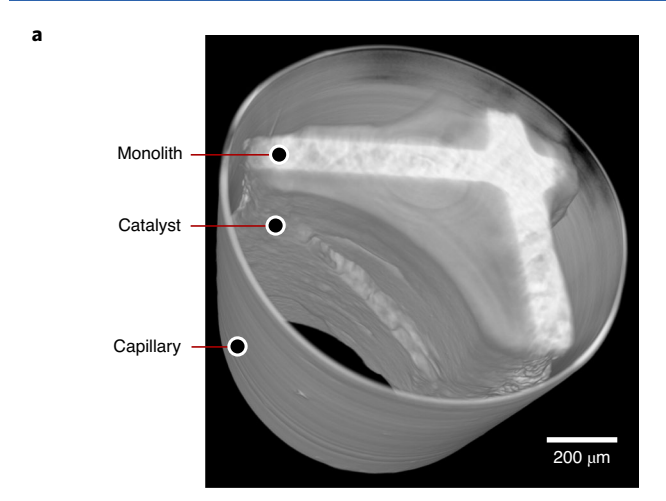
Influence of reaction temperature on chemical gradients. spectrotomography enabled identification co-localization of active metal sites throughout the entire sample. To illustrate this, an identical orthogonal slice was initially selected from the tomography volumes to compare the gradients present at different reaction temperatures (Fig. 3a-d). At 200 °C, XANES fitting showed a mixture of Cu(I) and Cu(II) coordinated with NH3 in the washcoat (Fig. 3a,e), while at the same time negligible NO conversion was recorded by mass spectrometry (Fig. 1b, Supplementary Discussion and Supplementary Fig. 16). These data confirm that the adsorption rate of NH3 in the washcoat was faster than the reaction rate. This led to an overall presence of NH₃ and, most probably, inhibition of the reaction due to strong adsorption of NH3 at low temperature^{9,11,12}. This inhibition effect was also described previously for iron-based zeolite SCR catalysts⁴⁶. Notably, the outer ROI (4-5) showed a gradual increase in the proportion of Cu(I) with adsorbed NH₃ compared to the more uniform composition of the inner washcoat (ROI 1-3) (Fig. 3a,e). Because reoxidation of Cu(I) to Cu(II) is considered to be a rate-limiting step⁴, the increased presence of Cu(I) at the washcoat exterior suggests that potential NH₃ inhibition effects are more pronounced there. At the same time, the washcoat interior underwent lower partial pressure of NO and NH₃ (due to reaction in the outer washcoat layer) and therefore a lower degree of NH₃ inhibition. At 200 °C this probably resulted in a higher SCR rate towards the washcoat interior, producing relatively more Cu(II) species visible in the inner washcoat regions (ROI 1-3). This

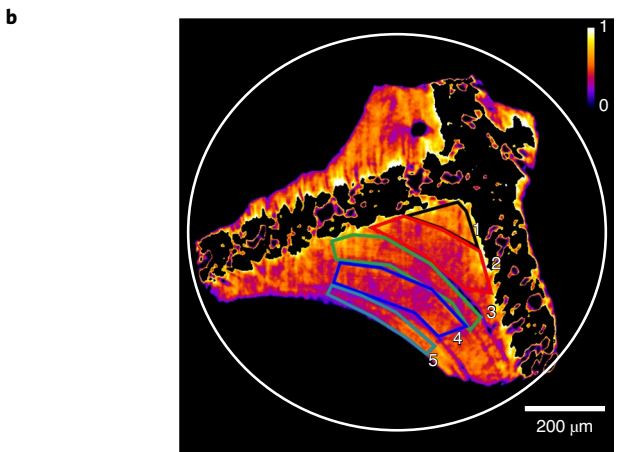
indicates that NO may have been partly consumed before reaching the inner washcoat (ROI 1–3), although N_2 detected by mass spectrometry was still negligible at this stage. Formation of water can also be expected during standard SCR, which at lower temperature (for example, 200 °C) can compete with NH $_3$ for adsorption on Cu sites, resulting in a higher fraction of Cu(II) species 9 . Here, due to low NO conversion at 200 °C, only limited water formation was expected. We therefore can begin to assemble a consistent picture of the reaction steps occurring within the washcoat using operando spectrotomography.

On heating to 300 °C a clear and striking gradient in oxidation state became visible, with greatly decreased Cu(II) content moving from the inner corner (ROI 1) to the washcoat exterior (ROI 5) (Fig. 3b,f). The more apparent gradients in Cu speciation at 300 compared to 200 °C can be explained by the relatively higher global reaction rate at the former (10% NO conversion) and the related reduced inhibitory effect of adsorbed NH3 at higher temperature9. Since the same environmental conditions were applied to the entire monolith sample, differences in the observed chemical state must be due to an additional effect. The strong gradients observed at 300 °C can therefore be interpreted as a direct, semi-quantitative visualization of the limitations to mass transport of NH₃ and NO reactant gases to the washcoat interior. The presence of such limitations is consistent with the increased formation of mainly Cu(I) species both with and without adsorbed NH3 in the outermost washcoat region (ROI 5)—that is, within 20 µm of the open channel (Fig. 3b,f). In effect, the greater the distance or diffusion length between a specific unit volume of the washcoat and the channel exterior, the less NO and NH3 reaches the inner ROI due to mass transport limitations and therefore the lower the reaction rate which would lead to Cu(I) formation.

At higher temperatures of 350 °C (Fig. 3c,g) to 400 °C (Fig. 3d,h), NO conversions remained around 10%. According to previous studies, a local conversion maximum would be expected to be reached at <300 °C for a typical Cu-SSZ-13 catalyst^{6,9}. The low maximum NO conversion (10%) observed here, together with the absence of a notable increase in NO conversion between 300 and 400 °C, is also consistent with the presence of severe mass transport limitations under the chosen gas flow conditions. Some portions of the catalyst washcoat were expected not to reach 100% conversion due to mass transport limitations of reactants to the active copper sites, while the relative temperature increase therefore had no appreciable effect on activity in these regions. At 350-400 °C the Cu(II) gradient first observed at lower temperatures was again clearly visible (Fig. 3a,b). However, in addition, the variation in local ammonia concentration at 350 °C compared to 400 °C also caused more apparent changes in XANES spectra (Fig. 3c,d), with an increased proportion of Cu(1)*NH3 moving towards the washcoat exterior (ROI 1-5). It is known that Cu-SSZ-13 SCR catalysts have a local minimum in NO conversion at around 350°C, the so-called seagull-shaped conversion curve⁴⁷, which is likely to coincide with more unconverted absorbed ammonia on Cu(I) species9,14,48. This is supported in spectrotomography by the absence of Cu(I) without ammonia at 350 °C (Fig. 3c,g) indicating total coverage of Cu(I)*NH3. In contrast, Cu(I) without ammonia was observed previously at 300 °C (Fig. 3b,f) and again at 400 °C (Fig. 3d,h). At temperatures of 350 °C and above, water is known to desorb from the zeolite while competition between water and NH3 for adsorption sites was previously found to be minimal9.

Following the apparent local activity minimum at 350°C, on heating to 400°C a complete and unambiguous reduction of Cu(II) to Cu(I) species (with and without NH₃) was observed in the outer areas of the washcoat ROI 4–5 (Fig. 3h). Due to high SCR rate, Cu(I)*NH₃ was observed predominantly in the outer region (ROI 5) with the highest local NH₃ concentration. On the other hand, the higher Cu(II) amount in the inner regions (ROI 1–2) is caused





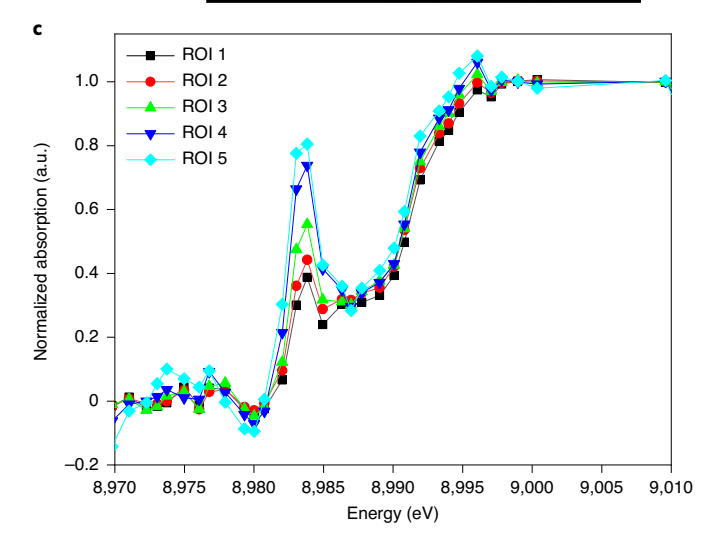


Fig. 2 | 3D view of the chemical gradient in a Cu-SSZ-13 washcoat. a, Tomography reconstruction of the entire monolith sample inside a 1-mm quartz capillary under SCR conditions. **b**, Orthogonal slice of the catalyst measured under SCR conditions at 350 °C; colour coding indicates the intensity of the XANES feature at 8,983 eV, showing the area of interest in ROI1-5. The cordierite monolith was thresholded and masked and did not affect washcoat analysis. **c**, Average normalized XANES spectra from voxels within ROI 1-5, corresponding to movement from the washcoat interior to exterior. a.u., arbitrary units.

by the lower NO concentration and thus lower SCR rate there. This indicates depletion of NO and NH₃ already in the outer regions, combined with relatively slow reactant diffusion to the washcoat

interior (mass transport limitations). Notably, no gradients were observed under the reference conditions measured (1,000 ppm NH $_3$ only, and 1,000 ppm NO with 7.8% $\rm O_2$), but rather a uniform composition of $\rm Cu(I)^*NH_3$ and $\rm Cu(II)$ was observed, respectively (Supplementary Discussion and Supplementary Fig. 14). This proves that the gradients observed during NH $_3$ -SCR are real observations and not a result of artefacts from data acquisition or tomographic reconstruction.

Insight into the NH3-SCR mechanism on structured catalysts. The use of our operando spectrotomography method offered detailed insights into a Cu-SSZ-13 washcoated monolith catalyst at work. For the first time, the consequences of mass transport limitations could be visualized in the form of chemical gradients in the structure of the Cu sites in Cu-SSZ-13. A stable NO conversion and N, yield were recorded at 300 °C and above (Fig. 1b) (at 200 °C, low conversion was observed; Supplementary Discussion), proving that the catalyst was captured in an active state and allowed structure and activity to be connected. This makes it possible to reinterpret earlier literature studies with differing explanations of copper active species. At the relatively low temperature of 200 °C, Cu(1)*NH₂ was present somewhat uniformly in the entire washcoat. This is consistent with the known strong inhibitory effect of NH, up to 300°C, which is weaker at higher temperatures9. However, in contrast to other studies³, Cu(I)*NH₃ or Cu(I) species were also found at 300-400 °C. In addition, complete reduction of the most active washcoat exterior regions to Cu(1) was observed at 400 °C. This is consistent with most currently proposed reaction mechanisms, which specify reoxidation of Cu(I) to Cu(II) as one rate-determining step at both low and elevated temperatures^{4,9}, coupled here with the presence of diffusion limitations to the inner washcoat. The latter may also explain why, in studies where mass transport is not optimal (for example, model disc-shaped catalysts), Cu(II) has been observed as the most abundant species at elevated temperatures^{3,45}. The gradients observed were also investigated as a function of washcoat thickness by studying different vertical positions of the monolith. Notably for thinner sections, Cu(I) was completely absent in favour of Cu(1)*NH₃ (Supplementary Discussion), reinforcing that sample thickness had a strong influence on NH3 adsorption under the cho-

Operando spectrotomography not only revealed that NH₃-SCR occurs non-uniformly within structured catalysts, but crucially could identify and locate specific chemical gradients linked to temperature and catalyst shape. This is in contrast to studies of NH₃-SCR on powder catalysts with conventional bulk XAS, where spatial variation and discrimination of Cu(1)*NH₃, Cu(1) and Cu(11) at different radial positions in the catalyst bed are physically not possible. A level of caution is therefore needed when interpreting results of operando studies on model systems. Without consideration of spatiotemporal effects or spatially resolved characterization tools, such studies may not be representative of the technical application. Furthermore it should be noted that conventional X-ray tomography, either ex situ or at a single energy, cannot produce the results shown here. An operando energy- and spatially resolved tomographic approach with quantitative activity data is absolutely essential to confirm that the reaction is occurring, to probe the chemical state (for example, using XAS) and to confirm the presence of gradients due to mass transport effects (rather than, for example, insufficient supply of reactants; Supplementary Note 1).

sen conditions and that operando spectrotomography is sufficiently

sensitive to detect these effects.

Conclusions

We demonstrate operando hard X-ray spectrotomography with XANES contrast as an effective characterization tool that can simultaneously perform spatially and energy-resolved 3D imaging, and identification of chemical states at micrometre-scale resolution using

ARTICLES NATURE CATALYSIS

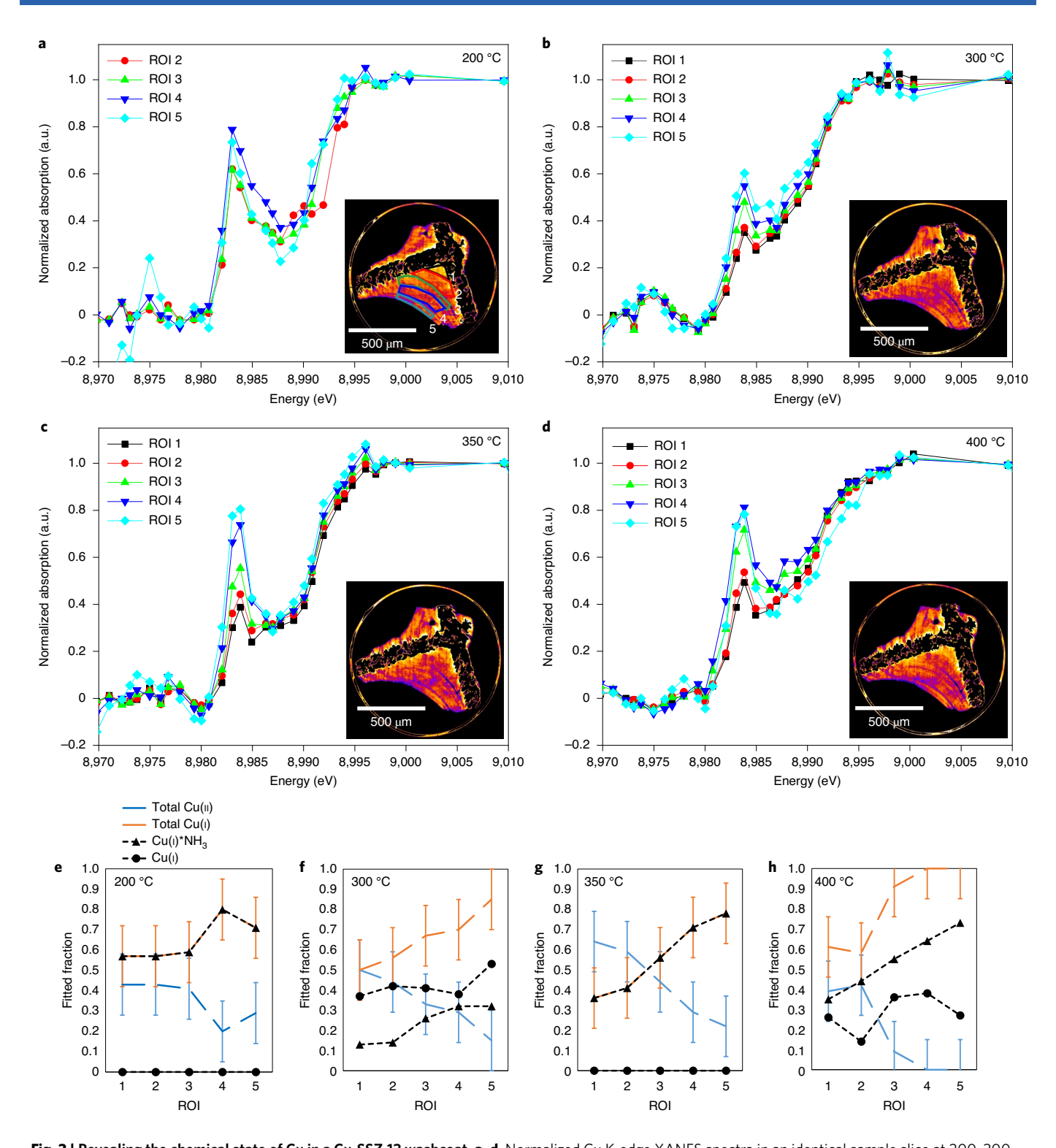


Fig. 3 | Revealing the chemical state of Cu in a Cu-SSZ-13 washcoat. a-d, Normalized Cu K-edge XANES spectra in an identical sample slice at 200, 300, 350 and 400 °C (a-d, respectively), showing visible gradients of the feature at 8,983 eV from ROI 1-5 (inset: fitted slice with colour coding corresponding to intensity of the XANES feature at 8,983 eV). e-h, Fitted fractions of Cu(i), Cu(i)*NH₃ and Cu(ii) in the XANES spectra at 200, 300, 350 and 400 °C (e-h, respectively) showing gradients from ROI 1-5. Error bars represent the maximum uncertainty reported by the linear combination analysis subroutine of the software package Athena 0.8.056. a.u., arbitrary units.

XAS. It is applicable to non-model catalyst systems under operando conditions, combined with quantitative catalytic performance data. Applying this method to NH₃-SCR over Cu-SSZ-13 washcoated monolith catalysts provides not only conclusive evidence of chemical gradients in Cu oxidation state and coordination environment

resulting from mass transport limitations in the catalyst washcoat, but demonstrates the potential to directly and semi-quantitatively image such gradients as a function of temperature and washcoat shape or thickness. Effectively, this enables observation of structure–activity relationships in complex heterogeneous catalytic

systems. The ability to visualize the effects of mass transport limitations in this way can improve our understanding of $\rm NH_3\text{-}SCR$ in technical systems and clarify the variation in observations found in the literature with respect to the reaction mechanism. However, performing operando tomographic imaging alone is not sufficient to investigate catalytic active sites during $\rm NH_3\text{-}SCR$: rather, a combined spectroscopic analysis such as XANES is required. The method is directly applicable to other transition or noble metal catalysed emission control processes and can be used to probe structure–activity relationships in 3D space, with relevance to catalyst synthesis, structure optimization and kinetic and multi-scale modelling.

Methods

Sample preparation. The Cu-SSZ-13 zeolite catalyst was prepared by liquid ion exchange of commercially purchased $NH_4\text{-}SSZ\text{-}13$ with a Si/Al ratio of 14. Cu exchange was carried out with a 0.005 M aqueous $\text{Cu}(\text{OAc})_2$ solution at room temperature for 24 h, after which the suspension was filtered, washed with deionized water and dried at 80 °C (ref. °). Afterwards the dried powder was calcined at 550 °C for 8 h in static air. X-ray fluorescence analysis confirmed a Cu loading of 1.8 wt%. A slurry of the calcined catalyst was prepared by mixing 5.43 g of Cu-SSZ-13 with 45 ml of deionized water and 1.43 g of binder (Ludox AS-40, colloidal silica solution) in a ball mill. The catalyst powder was applied to a rectangular cordierite honeycomb (cell density 400 per square inch, width 1 cm and length 2 cm) by dip coating and drying with a hot-air blower. This process was repeated until a total of 1.53 g cm $^{-3}$ washcoat was applied to the honeycomb. To finalize preparation of the honeycomb, it was calcined for 8 h at 550 °C in static air.

Operando spectrotomography set-up. The key to operando spectrotomography measurements was the development of a dedicated sample holder to combine operando spectroscopy and hard X-ray microtomography (Supplementary Methods, Supplementary Note 1 and Supplementary Figs. 1 and 2). The sample holder consisted of a quartz capillary (in this case, 1 mm diameter) as reactor, mounted vertically on a precision rotation stage (PRS-110, PI). The capillary was enclosed using epoxy glue in a support bracket ensuring free rotation, with gas connections at the top and bottom. A glassy carbon rod (HTW Hochtemperatur-Werkstoffe) was integrated to support the weight of the stainless steel gas connections and to reduce tension on the quartz capillary. The support rod is virtually transparent to hard X-rays at the Cu K-edge (8.979 keV), which was a key experimental advance in this study and did not negatively impact the tomography scans or the data reconstruction process (Supplementary Methods and Supplementary Fig. 3). The set-up is capable of maintaining micrometre-precision stability across the 180° rotational range required for tomography. The gas-dosing system consisted of mass flow controllers (Bronkhorst El-Flow), while the products were analysed using a mass spectrometer (Pfeiffer Vacuum OmniStar GSD-320) positioned downstream from the reactor. Two gas blowers (Leister LE Mini) were positioned on opposite sides of the capillary to provide even radial heat distribution to the sample. The gas blowers were controlled using custom LabVIEW scripts. The temperature was calibrated before measurement commenced and was checked at several time points during measurement using a type K thermocouple positioned close to the capillary exterior. The set-up therefore facilitates operando tomography measurements together with quantitative product sampling in a controlled gas and temperature environment. The set-up is portable and can be implemented at different microtomography beamlines (Supplementary Methods, Supplementary Note 1 and Supplementary Discussion).

Full-field XANES spectrotomography. A single monolith channel was cut out from the honeycomb structure with a razor and placed inside the spectrotomography sample holder. Measurements were performed at the microXAS beamline (Swiss Light Source, Paul Scherrer Institute, Switzerland), which is an insertion-device based beamline, using an undulator (U19) that serves as the radiation source. The incident full-field beam was tuned to a slightly larger size than the lateral cross-section of the capillary, covering an area of approximately 1.5×1.0 mm2. The beam size in the horizontal direction was tuned with a toroidal mirror placed about 17 m from the source and about 23 m from the sample position. A fixed-exit, double-crystal monochromator using a Si(111) crystal was used for energy selection of the X-rays. Full-field projections were recorded using an yttrium aluminium garnet scintillator doped with cerium, coupled to a tenfold objective and a charge-coupled device camera (pco.2000, 2,048 × 2,048 pixels, 7.4 µm pixel size, 6 e⁻ root mean square at 10 MHz). Flat-field projections (equivalent to incident intensity, I_0) were recorded regularly during measurement by moving the sample out of the beam position. Two-dimensional, full-field projections of the sample were recorded across a rotational range of 180° at a single energy to generate one tomogram. These projection series were repeated in sequence at a total of 51 energy points from 8.95 to 9.22 keV with variable step size (Supplementary Table 1), to produce Cu K-edge XANES data at each sampling point (detector pixel). The acquisition time for a complete projection series at all energy points was approximately 13h (Supplementary Note 1, Supplementary Methods and Supplementary Discussion).

Seven different measurement conditions were applied during spectrotomography measurements, including an ex situ scan under ambient conditions and sequential measurements under model standard SCR conditions (1,000 ppm NO, 1,000 ppm NH₃, 7.8% O₂ in He, total flow 50 ml min⁻¹) at four temperature points (200, 300, 350 and 400 °C). Two reference measurements were also performed, using 1,000 ppm NH₃ and 1,000 ppm NO with 7.8% O₂ in He, in both cases at 200 °C. Before spectrotomography scanning had begun, the sample was allowed to equilibrate for a minimum of 1 h under each condition. In the case of SCR measurements, these were performed only after stabilization of NO and N2 signals as observed by mass spectrometry, to ensure steady-state operation during the long tomography scans. The mass spectrometry data for NO and N₂ are shown and discussed in Supplementary Discussion and Supplementary Fig. 16. Water was not dosed as part of the standard SCR feed, due to the absence of heated gas lines and the small uniform heating zone of the gas blowers (Supplementary Methods). Formed water traces are expected to be relatively uniform along the reactor axis, due to low overall NO conversion at 200-400 °C.

Spectrotomography data processing. A full description of the data-processing procedure can be found in Supplementary Methods and Supplementary Fig. 3. The raw spectrotomography data consisted of full-field, two-dimensional projection series across a 180° rotation range. Each projection series contained the carbon support rod at several angles, which was firstly subtracted as a background feature to produce corrected projection series containing only the sample and capillary. To compensate for fluctuation in beam intensity and sample movement, alignment was performed first for energy series at each projection angle followed by a second alignment of projection series at each rotational angle. Individual sinograms were then generated for each horizontal line on the aligned projection series at each energy point, followed by reconstruction of the sinograms using the simultaneous iterative reconstruction algorithm of the ASTRA Python library49. The resulting 3D volumes provide a non-invasive, 3D, spatially resolved view of the monolith interior, resolved by both energy and X-ray absorbance, whereby each individual sampling point contains a full XANES spectrum. The resulting datasets can be considered multidimensional with at least five dimensions, even before considering time, temperature and catalytic activity as additional parameters.

Linear combination analysis of ROI-averaged XANES spectra. Linear combination analysis of XANES spectra in the region 8,979.5-8,992.5 eV (rising-edge region) was used to determine the state of Cu in the corresponding parts of the washcoat (Supplementary Table 2 and Supplementary Discussion). The spectra extracted were an average of individual pixel contributions contained within each ROI, including 3,132, 8,559, 8,181, 8,919 and 3,786 pixels for ROI 1-5, respectively. Before linear combination analysis, the XANES spectra acquired in each ROI were normalized using the pre-edge region from -33 to -3 eV and post-edge region from +15 to +27 eV. Such short ranges were chosen due to limited density of scanning points (51 in total from 8,950 to 9,220 eV) as a result of time constraints. ATHENA software from the IFFEFIT package was used for data analysis50. As references, the spectra of hydrated Cu(II) (which was not required and exerted no effect on the fit results at 350 and 400 °C, in accordance with previous work¹⁰) and dehydrated Cu(II) species were used (spectra of Cu(II) with or without adsorbed ammonia were too similar to distinguish in our case)14. It is important to note that the quality of fitting for ROIs with higher Cu(II) content was generally worse than for other species. This most probably arose from the presence of Cu(II) with adsorbed NH3 species for which a reference was not available, due to similarity of their spectra to other Cu(II) references¹⁴. Cu(I)*NH₃ and Cu(I) references were obtained from operando QEXAFS data previously measured on a powdered Cu-SSZ-13 catalyst using multivariate curve resolution-alternating least-squares method (Supplementary Discussion)9,10. To check the fitting procedure for robustness, we also performed fits using internal reference spectra obtained in NH₃ (as a reference of Cu(1)*NH₃) and in NO+O₂ (as a reference of Cu(II)) at 200 °C, with this approach leading to the same observed trends (Supplementary Discussion and Supplementary Fig. 14). The reference spectra were normalized in the same way as the XANES spectrotomography data. During fitting, energy adjustment within 1 eV was allowed for the experimental spectra while the energy scale of the reference spectra was fixed. The energy adjustment was performed because the references were measured by standard transmission XAS together with the Cu foil reference sample for proper energy scale calibration, while for the spectrotomography data the energy scale stability could be measured only at regular intervals between rotational series. In addition, the energy resolution between conventional XAS and spectrotomography may be slightly different due to variation in instrumentation and beam size. Altogether, the fits included 13 data points and three to four fitted variables (two to three for weights and one for the energy shift). The misfit (ρ) is defined as $\Sigma({\rm data-fit})^2/\Sigma({\rm data})^2$, and the error bars for the calculated weights are within ±0.15. Fitted spectra and residuals are shown in Supplementary Discussion and Supplementary Figs. 4-9.

Data availability

Raw data were generated at the Swiss Light Source of the Paul Scherrer Institut (Switzerland). The collected and cleaned imaging data acquired before tomographic reconstruction that support the findings of this study are stored in

ARTICLES NATURE CATALYSIS

KITopen, the central repository of the Karlsruhe Institute of Technology, and are freely available with the following DOIs: 200 °C dataset, https://doi.org/10.5445/IR/1000122874; 300 °C dataset, https://doi.org/10.5445/IR/1000122890; 350 °C dataset, https://doi.org/10.5445/IR/1000122893; NH $_3$ reference dataset, https://doi.org/10.5445/IR/1000122894; NO reference dataset, https://doi.org/10.5445/IR/1000122895. Additional data, including reconstructed and treated spectrotomography datasets, are available from the authors upon reasonable request. Source Data for Figs. 1–3 are provided with the paper.

Received: 27 May 2020; Accepted: 11 November 2020; Published online: 14 December 2020

References

- Beale, A. M., Gao, F., Lezcano-Gonzalez, I., Peden, C. H. F. & Szanyi, J. Recent advances in automotive catalysis for NO_x emission control by small-pore microporous materials. *Chem. Soc. Rev.* 44, 7371–7405 (2015).
- Borfecchia, E. et al. Cu-CHA—a model system for applied selective redox catalysis. Chem. Soc. Rev. 47, 8097–8133 (2018).
- Lomachenko, K. A. et al. The Cu-CHA deNO_x catalyst in action: temperature-dependent NH₃-assisted selective catalytic reduction monitored by operando XAS and XES. J. Am. Chem. Soc. 138, 12025–12028 (2016).
- Janssens, T. V. W. et al. A consistent reaction scheme for the selective catalytic reduction of nitrogen oxides with ammonia. ACS Catal. 5, 2832–2845 (2015).
- Bates, S. A. et al. Identification of the active Cu site in standard selective catalytic reduction with ammonia on Cu-SSZ-13. J. Catal. 312, 87–97 (2014).
- Günter, T. et al. Structural snapshots of the SCR reaction mechanism on Cu-SSZ-13. Chem. Commun. 51, 9227–9230 (2015).
- Günter, T. et al. The SCR of NO_x with NH₃ examined by novel X-ray emission and X-ray absorption methods. *Top. Catal.* 59, 866–874 (2016).
- Paolucci, C. et al. Dynamic multinuclear sites formed by mobilized copper ions in NO_x selective catalytic reduction. *Science* 357, 898–903 (2017).
- Fahami, A. R. et al. The dynamic nature of Cu sites in Cu-SSZ-13 and the origin of the seagull NO_x conversion profile during NH₃-SCR. React. Chem. Eng. 4, 1000–1018 (2019).
- Kerkeni, B. et al. Copper coordination to water and ammonia in CuII-exchanged SSZ-13: atomistic insights from DFT calculations and in situ XAS experiments. J. Phys. Chem. C 122, 16741–16755 (2018).
- Auvray, X. et al. Local ammonia storage and ammonia inhibition in a monolithic copper-beta zeolite SCR catalyst. Appl. Catal. B 126, 144–152 (2012).
- 12. Marberger, A. et al. Time-resolved copper speciation during selective catalytic reduction of NO on Cu-SSZ-13. *Nat. Catal.* 1, 221–227 (2018).
- Greenaway, A. G. et al. Detection of key transient Cu intermediates in SSZ-13 during NH₃-SCR deNO_x by modulation excitation IR spectroscopy. *Chem. Sci.* 11, 447–455 (2020).
- Clark, A. H. et al. Selective catalytic reduction of NO with NH₃ on Cu-SSZ-13: deciphering the low- and high-temperature rate-limiting steps by transient XAS experiments. *ChemCatChem* 12, 1429–1435 (2020).
- Grunwaldt, J.-D., Wagner, J. B. & Dunin-Borkowski, R. E. Imaging catalysts at work: a hierarchical approach from the macro- to the meso- and nano-scale. ChemCatChem 5, 62–80 (2013).
- Gänzler, A. M. et al. Unravelling the different reaction pathways for low temperature CO oxidation on Pt/CeO₂ and Pt/Al₂O₃ by spatially resolved structure–activity correlations. J. Phys. Chem. Lett. 10, 7698–7705 (2019).
- Andrews, J. C. & Weckhuysen, B. M. Hard X-ray spectroscopic nano-imaging of hierarchical functional materials at work. *ChemPhysChem* 14, 3655–3666 (2013).
- Goguet, A., Stewart, C., Touitou, J. & Morgan, K. in Spatially Resolved Operando Measurements in Heterogeneous Catalytic Reactors Vol. 50 (eds Dixon, A. G. & Deutschmann, O.) 131–160 (Elsevier, 2017).
- Dong, Y., Korup, O., Gerdts, J., Roldán Cuenya, B. & Horn, R. Microtomography-based CFD modeling of a fixed-bed reactor with an open-cell foam monolith and experimental verification by reactor profile measurements. *Chem. Eng. J.* 353, 176–188 (2018).
- Jurtz, N., Kraume, M. & Wehinger, G. D. Advances in fixed-bed reactor modeling using particle-resolved computational fluid dynamics (CFD). Rev. Chem. Eng. 35, 139–190 (2019).
- Buurmans, I. L. C. & Weckhuysen, B. M. Heterogeneities of individual catalyst particles in space and time as monitored by spectroscopy. *Nat. Chem.* 4, 873–886 (2012).
- Urakawa, A. & Baiker, A. Space-resolved profiling relevant in heterogeneous catalysis. *Top. Catal.* 52, 1312–1322 (2009).
- Beale, A. M., Jacques, S. D. M. & Weckhuysen, B. M. Chemical imaging of catalytic solids with synchrotron radiation. *Chem. Soc. Rev.* 39, 4656–4672 (2010).
- 24. Sanchez, D. F. et al. 2D/3D microanalysis by energy dispersive X-ray absorption spectroscopy tomography. *Sci. Rep.* 7, 16453 (2017).

 Ihli, J. et al. A three-dimensional view of structural changes caused by deactivation of fluid catalytic cracking catalysts. Nat. Commun. 8, 809 (2017).

- Sheppard, T. L. et al. In situ multimodal 3D chemical imaging of a hierarchically structured Core@Shell catalyst. J. Am. Chem. Soc. 139, 7855–7863 (2017).
- 27. Weker, J. N., Huang, X. & Toney, M. F. In situ X-ray-based imaging of nano materials. *Curr. Op. Chem. Eng.* 12, 14–21 (2016).
- Price, S. W. T. et al. Chemical imaging of single catalyst particles with scanning μ-XANES-CT and μ-XRF-CT. Phys. Chem. Chem. Phys. 17, 521–529 (2015).
- Becher, J. et al. Mapping the pore architecture of structured catalyst monoliths from nanometer to centimeter scale with electron and X-ray tomographies. J. Phys. Chem. C 123, 25197–25208 (2019).
- Hofmann, G. et al. Aging of a Pt/Al₂O₃ exhaust gas catalyst monitored by quasi in situ X-ray micro computed tomography. RSC Adv. 5, 6893–6905 (2015).
- Meirer, F. et al. Mapping metals incorporation of a whole single catalyst particle using element specific X-ray nanotomography. J. Am. Chem. Soc. 137, 102–105 (2015).
- Bossers, K. W. et al. Correlated X-ray ptychography and fluorescence nano-tomography on the fragmentation behavior of an individual catalyst particle during the early stages of olefin polymerization. *J. Am. Chem. Soc.* 142, 3691–3695 (2020).
- Price, S. W. T. et al. Chemical imaging of Fischer–Tropsch catalysts under operating conditions. Sci. Adv. 3, e1602838 (2017).
- 34. Senecal, P. et al. Real-time scattering-contrast imaging of a supported cobalt-based catalyst body during activation and Fischer–Tropsch synthesis revealing spatial dependence of particle size and phase on catalytic properties. ACS Catal. 7, 2284–2293 (2017).
- Cats, K. et al. Active phase distribution changes within a catalyst particle during Fischer–Tropsch synthesis as revealed by multi-scale microscopy. Catal. Sci. Technol. 6, 4438–4449 (2016).
- Matras, D. et al. Operando and postreaction diffraction imaging of the La–Sr/ CaO catalyst in the oxidative coupling of methane reaction. *J. Phys. Chem. C* 123, 1751–1760 (2019).
- Vamvakeros, A. et al. Real time chemical imaging of a working catalytic membrane reactor during oxidative coupling of methane. *Chem. Commun.* 51, 12752–12755 (2015).
- 38. Vamvakeros, A. et al. 5D operando tomographic diffraction imaging of a catalyst bed. *Nat. Commun.* **9**, 4751 (2018).
- Schmidt, J. E., Oord, R., Guo, W., Poplawsky, J. D. & Weckhuysen, B. M. Nanoscale tomography reveals the deactivation of automotive copper-exchanged zeolite catalysts. *Nat. Commun.* 8, 1666 (2017).
- Schmidt, J. E. et al. Probing the location and speciation of elements in zeolites with correlated atom probe tomography and scanning transmission X-ray microscopy. *ChemCatChem* 11, 488–494 (2019).
- Paolucci, C. et al. Isolation of the copper redox steps in the standard selective catalytic reduction on Cu-SSZ-13. Angew. Chem. Int. Ed. 53, 11828–11833 (2014).
- Alayon, E. M. C., Nachtegaal, M., Kleymenov, E. & van Bokhoven, J. A. Determination of the electronic and geometric structure of Cu sites during methane conversion over Cu-MOR with X-ray absorption spectroscopy. *Micropor. Mesopor. Mater.* 166, 131–136 (2013).
- Zhang, R. & McEwen, J.-S. Local environment sensitivity of the Cu K-edge XANES features in Cu-SSZ-13: analysis from first-principles. *J. Phys. Chem. Lett.* 9, 3035–3042 (2018).
- Bendrich, M., Scheuer, A., Hayes, R. E. & Votsmeier, M. Unified mechanistic model for standard SCR, fast SCR, and NO₂ SCR over a copper chabazite catalyst. Appl. Catal. B 222, 76–87 (2018).
- Giordanino, F. et al. Interaction of NH₃ with Cu-SSZ-13 catalyst: a complementary FTIR, XANES, and XES study. *J. Phys. Chem. Lett.* 5, 1552–1559 (2014).
- Doronkin, D. E. et al. Operando spatially- and time-resolved XAS study on zeolite catalysts for selective catalytic reduction of NO_x by NH₃. *J. Phys. Chem. C* 118, 10204–10212 (2014).
- Gao, F., Mei, D., Wang, Y., Szanyi, J. & Peden, C. H. F. Selective catalytic reduction over Cu/SSZ-13: linking homo- and heterogeneous catalysis. *J. Am. Chem. Soc.* 139, 4935–4942 (2017).
- Gao, F. et al. Understanding ammonia selective catalytic reduction kinetics over Cu/SSZ-13 from motion of the Cu ions. J. Catal. 319, 1–14 (2014).
- 49. van Aarle, W. et al. Fast and flexible X-ray tomography using the ASTRA toolbox. *Opt. Express* 24, 25129–25147 (2016).
- Ravel, B. & Newville, M. ATHENA, ARTEMIS, HEPHAESTUS: data analysis for X-ray absorption spectroscopy using IFEFFIT. J. Synchrotron Radiat. 12, 537–541 (2005).

Acknowledgements

This work was supported by the German Federal Ministry of Education and Research (BMBF) projects MicTomoCat (no. 05K16VK1) and COSMIC (no. 05K19VK4), and the German Research Foundation project (no. GR 3987/5-1). Spectrotomography

experiments were performed at beamline microXAS of the Swiss Light Source. We acknowledge the Paul Scherrer Institut, Villigen, Switzerland for provision of synchrotron radiation beamtime at beamline microXAS, and thank M. Birri, B. Meyer and D. Grolimund for technical assistance and scientific discussions. Additional energy-dispersive spectrotomography experiments were performed on beamline ID24 at the European Synchrotron Radiation Facility, Grenoble, France. We thank F. Perrin and S. Pasternak for technical assistance. Furthermore we thank T. Bergfeldt (IAM-AWP, Karlsruhe Institute of Technology) for elemental analysis of the ion-exchanged zeolite; we thank M. Casapu from the Karlsruhe Institute of Technology for discussions on NH₃-SCR, P. Lott for assistance during beamtime and D. Yuda for assistance with design of the reaction set-up. D.Z. additionally thanks the Deutsche Bundesstiftung Umwelt for the scholarship provided. T.L.S. thanks the BMBF and project COSMIC for funding.

Author contributions

T.L.S., D.M.M., D.E.D. and J.-D.G. conceived and designed the experiments. J.B. and T.L.S. designed the spectrotomography set-up. J.B. and D.Z. synthesized the materials. J.B., D.F.S., D.E.D., D.M.M., S.P., J.-D.G. and T.L.S. contributed to preparation of beamtime proposals for access to synchrotron radiation. J.B., D.F.S., D.E.D., D.Z., D.M.M., S.P. and T.L.S. performed the experiments and acquired the data. D.F.S. and J.B. prepared code for processing of the raw data. J.B., D.F.S., D.E.D. and T.L.S performed

analysis of the processed data and, with J.-D.G., interpreted the data. J.B., T.L.S. and D.E.D. drafted the manuscript, and all authors contributed to revision of the manuscript. J.-D.G. and T.L.S. were responsible for acquisition of funding.

Competing interests

The authors declare no competing interests.

Additional information

Supplementary information is available for this paper at https://doi.org/10.1038/s41929-020-00552-3.

Correspondence and requests for materials should be addressed to J.-D.G. or T.L.S.

Peer review information *Nature Catalysis* thanks Jianjun Chen and the other, anonymous, reviewer(s) for their contribution to the peer review of this work.

Reprints and permissions information is available at www.nature.com/reprints.

Publisher's note Springer Nature remains neutral with regard to jurisdictional claims in published maps and institutional affiliations.

© The Author(s), under exclusive licence to Springer Nature Limited 2020